2016

Stress-dependent ultrasonic scattering in polycrystalline materials

Christopher M. Kube
University of Nebraska–Lincoln, ckube@huskers.unl.edu

Joseph A. Turner
University of Nebraska–Lincoln, jaturner@unl.edu

Stress-dependent ultrasonic scattering in polycrystalline materials

Christopher M. Kube[a] and Joseph A. Turner
Department of Mechanical and Materials Engineering, W342 Nebraska Hall, University of Nebraska–Lincoln, Lincoln, Nebraska 68588-0526, USA

(Received 25 September 2015; revised 17 December 2015; accepted 24 December 2015; published online 12 February 2016)

Stress-dependent elastic moduli of polycrystalline materials are used in a statistically based model for the scattering of ultrasonic waves from randomly oriented grains that are members of a stressed polycrystal. The stress is assumed to be homogeneous and can be either residual or generated from external loads. The stress-dependent elastic properties are incorporated into the definition of the differential scattering cross-section, which defines how strongly an incident wave is scattered into various directions. Nine stress-dependent differential scattering cross-sections or scattering coefficients are defined to include all possibilities of incident and scattered waves, which can be either longitudinal or (two) transverse wave types. The evaluation of the scattering coefficients considers polycrystalline aluminum that is uniaxially stressed. An analysis of the influence of incident wave propagation direction, scattering direction, frequency, and grain size on the stress-dependency of the scattering coefficients follows. Scattering coefficients for aluminum indicate that ultrasonic scattering is much more sensitive to a uniaxial stress than ultrasonic phase velocities. By developing the stress-dependent scattering properties of polycrystals, the influence of acoustoelasticity on the amplitudes of waves propagating in stressed polycrystalline materials can be better understood. This work supports the ongoing development of a technique for monitoring and measuring stresses in metallic materials.
[http://dx.doi.org/10.1121/1.4941253]

[ANN] Pages: 811–824

I. INTRODUCTION

Acoustoelasticity is most often associated with the phase velocity of a small-amplitude acoustic wave propagating in a stressed material. It is well-known that the measurement of the transit time of a wave over a fixed distance of material can be correlated with the material stresses present. Acoustoelastic methods based on phase velocity variations have found a variety of applications in the nondestructive evaluation of materials.[1–6] Crecraft exploited the birefringence of shear waves to estimate residual stresses.[1] Egle and Bray used acoustoelasticity to measure the stress-dependent elastic properties of steel used in railway applications.[2] Kino and co-workers developed a precise measurement system for the evaluation of residual and applied stresses.[3,4] King and Fortunko[5] and Thompson *et al.*[6] used horizontally polarized shear waves to perform texture independent measurements of residual stress. Acoustoelastic techniques have also been used to determine the third-order elastic constants and anharmonic properties of crystalline materials.[7–10] These applications along with the theoretical development of the underlying physics have reached a high level of maturity over the past decades. Reviews on the topic of acoustoelasticity are given by Green,[11] Pao *et al.*,[12] and Hirao and Ogi.[13]

While much progress has been made in acoustoelasticity, the effects of material stresses on the amplitudes of elastic waves has received less attention. Hikata *et al.*[14] demonstrated that dislocations in materials absorb a portion of the wave's energy at a rate that is dependent on the material's stress state. Hikata and co-workers[15–17] observed the influence of an applied load on the velocity and attenuation of an elastic wave in single-crystals, which was attributed to dislocation behavior. More recently, Ogi *et al.*[18] observed that acoustoelasticity theory did not agree with experimental phase velocity measurements on polycrystalline copper. They attributed a dual influence of dislocations and acoustoelasticity on the stress-dependent phase velocity.[13,18] They also observed the attenuation dependence of longitudinal and shear waves in the polycrystalline copper sample under compressive and tensile loads.[13,18] Like previous researchers,[14] they attributed the stress-dependence of the attenuation coefficient to the absorption of ultrasonic energy by the stress-dependent behavior of the dislocations.[13,18]

In polycrystalline materials, like polycrystalline copper, scattering from grain boundaries is the primary source of attenuation for elastic waves at ultrasonic frequencies. Thus, the measured baseline stress-free attenuation value is dominated by losses caused by grain scattering rather than absorption. Dislocations can bow, break-free, and re-pin as they respond to changes of an external loading. These events cause the dislocations to absorb ultrasonic energy at different rates which may result in a change in the observed attenuation coefficient. The evolution of the attenuation coefficient

[a]Present address: Army Research Laboratory, Vehicle Technology Directorate, Mechanics Division, 4603 Flare Loop, Aberdeen Proving Ground, MD 21005-5069, USA. Electronic mail: ckube@huskers.unl.edu

during loading is discussed in the results of Ogi *et al.*[18] However, the influence of dislocations is only one of the factors that may change attenuation during loading of polycrystalline materials. The scattering from grain boundaries is also stress-dependent, which is a result of the stress-dependent or acoustoelastic properties of the individual grains composing the polycrystal. Turner and Ghoshal first formulated the second-order elastic properties of stressed polycrystals that are needed to describe ultrasonic grain scattering.[19] Kube *et al.* experimentally demonstrated the influence of applied loads on ultrasonic backscatter.[20,21] More recently, Kube and Turner[22] reformulated the stress-dependent elastic properties of the polycrystal to allow for residual stresses and provided a correction to Turner and Ghoshal[19] (see Appendix A of Kube and Turner[22]).

In this article, the stress-dependent elastic moduli[22] of the individual grains composing the polycrystal are used to model the influence of material stress on ultrasonic (bulk wave) scattering from grain boundaries. In Sec. II, the stress-dependent scattering coefficients are defined. These scattering coefficients represent the fraction of energy from an incident wave scattered into a given direction. An incident wave can be one of three possible modetypes that are either longitudinal or two distinctly polarized shear modes. Scattered waves can be mode-converted into different modetypes. Thus, nine unique scattering coefficients can be defined, which cover all combinations of incident and scattered longitudinal and shear wave modes.

Material stress can influence each of the nine scattering coefficients differently, with some coefficients having a stronger sensitivity to stress. Additionally, the sensitivity to material stresses depends on the propagation and polarization directions of the incident and scattered waves. Thus, a vast number of scattering configurations are possible. Section III analyzes the dependence of a uniaxial stress on the scattering coefficients for some possible experimental configurations. In addition, the influence of frequency and grain size on the stress-dependency is given. These results indicate that scattering amplitudes are far more sensitive to material stress than phase velocities.

This work provides the connection between the stress-dependent elastic properties, which is foundational to acoustoelasticity, and the stress-dependent scattering losses of an ultrasonic wave due to scattering from grain boundaries. Experimentally measuring stresses from the scattered response is the primary future direction of this work. This scattered response is obtained by analyzing the average incoherent scattering present in a collection of ultrasonic waveforms using either an ultrasonic pulse/echo[23,24] or pitch/catch[25] transducer configuration. In the absence of defects or other inhomogeneities, the scattered response is dominated by scattering from grain boundaries. This effect is especially true when the scattering is measured at early times so that the attenuation of the incident and scattered wave is negligible. Unlike measurements of phase velocities[18] or attenuation coefficients, grain scattering is weakly dependent on effects from dislocation behavior because of the smaller length scales of dislocations. There is also strong agreement between theoretical backscatter models and experimental scattering measurements.[23–25] Thus, no decoupling of competing effects[18] is necessary when correlating material stresses to ultrasonic scattering.

II. THEORY

An ultrasonic wave transmitted into a polycrystalline material scatters at the boundaries or interfaces between adjacent grains. The magnitude of the scattering depends on the variation of the elastic moduli throughout the polycrystal, which results from the spatial distribution of grain orientations. In this article, the variation of the elastic moduli is assumed to be stress-dependent and defined by the statistical covariance of the stress-dependent elastic moduli of the individual grains. The stress-dependent covariance is an eighth-rank tensor $\boldsymbol{\Xi}$ that was defined in the previous work of Kube.[26] The derivation of $\boldsymbol{\Xi}$ was based on the constitutive relation derived by Man and co-workers, which is valid for both residual and mechanical stresses.[27–32] The components of $\boldsymbol{\Xi}$ were shown to be quadratic with respect to the magnitude of the components of the Cauchy stress tensor, e.g., $\Xi_{33}^{33} = K_0 + K_1\sigma_{33} + K_2\sigma_{33}^2$ where the coefficients K_0, K_1, and K_2 are combinations of ensemble averaged second- and third-order single crystal elastic constants.[33] These coefficients are unique for each of the possible components of $\boldsymbol{\Xi}$. Analytical expressions of K_0, K_1, and K_2 are given in the Appendix for the component Ξ_{33}^{33} assuming a uniaxial stress σ_{33}. From the single-crystal elastic constants given in Table I for aluminum, the 44 independent components of $\boldsymbol{\Xi}$ were calculated and given in Table II. The procedure for calculating these independent components is given elsewhere.[22]

Once all of the components of $\boldsymbol{\Xi}$ are known, a differential scattering coefficient Ω can then be formed from inner products of $\boldsymbol{\Xi}$ with the propagation and displacement vectors of the incident and scattered waves. Ω defines the differential scattering cross-section of the scattered wave field from an ensemble of grains contained within the ultrasonic beam. Several derivations of the stress-independent scattering coefficients can be found in previous literature.[23–25,36–40] Rose[36,37] and Margetan[39] derived scattering coefficients by using reciprocal relations between the power of the incident and scattered wave fields. Turner obtained scattering coefficients within his models of radiative transfer of ultrasound.[38] Ghoshal *et al.* obtained scattering coefficients for a model of the single-scattered response by deriving the Wigner distribution functions of the incident and scattered wave fields.[23,24] Hu *et al.* extended the Wigner distribution definitions to account for a mode-converted scattered shear wave from an incident longitudinal wave.[25] Hirsekorn derived scattering coefficients by considering the ensemble averaged response of the power flux density from a distribution of spherical scatterers.[40] The various derivations reduce to the

TABLE I. Second- and third-order single-crystal elastic constants for aluminum (in GPa) (see Refs. 34, 35).

	c_{11}	c_{12}	c_{44}	c_{111}	c_{112}	c_{123}	c_{144}	c_{155}	c_{456}
Al	107	61	28	−1080	−315	36	−23	−340	−30

TABLE II. Stress-dependent covariance tensor components for aluminum (single-crystal elastic constants given in Table I) defined in terms of the coefficients K_0 (GPa^2), K_1 (GPa), and K_2 (dimensionless units).

	Ξ_{11}^{11}	Ξ_{11}^{12}	Ξ_{11}^{13}	Ξ_{11}^{66}	Ξ_{11}^{55}	Ξ_{11}^{22}	Ξ_{11}^{23}	Ξ_{11}^{44}	Ξ_{11}^{33}	Ξ_{16}^{16}	Ξ_{16}^{26}
K_0	3.048	−1.524	−1.524	−1.524	−1.524	1.143	0.381	0.381	1.143	1.905	−1.429
K_1	1.161	−0.798	0.038	−0.714	0.065	0.597	0.10	−0.011	−0.438	0.847	−0.706
K_2	0.907	−0.197	−0.655	−0.187	−0.650	0.103	0.075	0.059	0.544	0.370	−0.169
	Ξ_{16}^{36}	Ξ_{16}^{45}	Ξ_{15}^{15}	Ξ_{15}^{46}	Ξ_{15}^{25}	Ξ_{15}^{35}	Ξ_{12}^{12}	Ξ_{12}^{13}	Ξ_{12}^{66}	Ξ_{12}^{55}	Ξ_{12}^{33}
K_0	−0.476	−0.476	1.905	−0.476	−0.476	−1.429	1.714	−0.190	1.714	−0.190	0.381
K_1	−0.016	0.019	−0.016	−0.032	−0.137	0.528	0.751	0.098	0.779	0.084	−0.295
K_2	−0.183	−0.178	0.753	−0.037	−0.034	−0.729	0.298	−0.115	0.291	−0.111	0.256
	Ξ_{14}^{14}	Ξ_{14}^{56}	Ξ_{14}^{34}	Ξ_{13}^{13}	Ξ_{13}^{66}	Ξ_{13}^{55}	Ξ_{13}^{23}	Ξ_{13}^{44}	Ξ_{13}^{33}	Ξ_{66}^{66}	Ξ_{66}^{55}
K_0	0.952	0.952	−0.476	1.714	−0.190	1.714	−0.190	−0.190	−1.524	1.714	−0.190
K_1	−0.007	0.027	0.269	−0.585	−0.014	−0.599	−0.148	−0.023	1.133	0.806	−0.028
K_2	0.281	0.273	−0.275	0.847	−0.088	0.841	0.059	0.037	−1.002	0.300	−0.092
	Ξ_{66}^{33}	Ξ_{56}^{56}	Ξ_{56}^{34}	Ξ_{36}^{36}	Ξ_{36}^{45}	Ξ_{55}^{55}	Ξ_{55}^{44}	Ξ_{55}^{33}	Ξ_{45}^{45}	Ξ_{35}^{35}	Ξ_{33}^{33}
K_0	0.381	0.952	−0.476	0.952	0.952	1.714	−0.190	−1.524	0.952	1.905	3.048
K_1	−0.072	0.062	0.129	−0.218	−0.288	−0.613	0.103	1.022	−0.358	−1.297	−3.066
K_2	0.144	0.275	−0.227	0.394	0.402	0.845	0.015	−0.946	0.415	1.174	2.406

same result for the different possible scattering coefficients. Thus, the present article does not repeat or endorse a single approach. Based on results from previous derivations,[23–25,36–40] the scattering coefficient is written as

$$\Omega^{\mathrm{I}\to\mathrm{S}} = \frac{v^{-3}v'^{-5}}{2\pi\rho^2} \frac{L^3\,\Xi_{ijkl}^{\alpha\beta\gamma\delta}\hat{e}_i\hat{n}_j\hat{e}'_k\hat{n}'_l\hat{e}_\alpha\hat{n}_\beta\hat{e}'_\gamma\hat{n}'_\delta}{\left[\omega^{-2}+L^2\left(v^{-2}+v'^{-2}-2v^{-1}v'^{-1}\hat{n}_p\hat{n}'_p\right)\right]^2}, \tag{1}$$

where the primed notation denotes variables corresponding to the scattered wave. The superscripts I and S indicate the incident and scattered mode types. For example, $\Omega^{\mathrm{qP}\to\mathrm{qSV}}$ defines the scattered power of a quasi-shear vertical wave (qSV) scattered from an incident quasi-longitudinal wave (qP).[41] In this example, the qP-wave propagates in the direction $\hat{\mathbf{n}}$, with displacement $\hat{\mathbf{e}}$, and phase velocity v while the scattered qSV-wave propagates in the direction $\hat{\mathbf{n}}'$, with displacement $\hat{\mathbf{e}}'$ and phase velocity v'. The remaining variables are the density and average grain radius of the polycrystal given by the variables ρ and L, respectively. The inner product $\Xi_{ijkl}^{\alpha\beta\gamma\delta}\hat{e}_i\hat{n}_j\hat{e}'_k\hat{n}'_l\hat{e}_\alpha\hat{n}_\beta\hat{e}'_\gamma\hat{n}'_\delta$ is evaluated using the components of $\Xi_{ijkl}^{\alpha\beta\gamma\delta}$, which were derived for any stress state $\boldsymbol{\sigma}$ and given explicitly for a uniaxial stress σ_{33} in previous work.[26] For brevity, this article considers the same case with a single non-zero stress component σ_{33}. In this case, the stress-dependent phase velocities are written in closed-form as[42]

$$\begin{aligned} v_{\mathrm{qP}} &= \rho^{-1/2}[\Lambda_{33}^0(\kappa_1\sin^2\theta+\chi+1)+\sigma_{33}\cos^2\theta]^{1/2}, \\ v_{\mathrm{qSV}} &= \rho^{-1/2}[\Lambda_{44}^0+\Lambda_{33}^0(\kappa_1\sin^2\theta-\chi)+\sigma_{33}\cos^2\theta]^{1/2}, \text{ and} \\ v_{\mathrm{SH}} &= \rho^{-1/2}[\Lambda_{44}^0(2\kappa_2\sin^2\theta+1)+\sigma_{33}\cos^2\theta]^{1/2}, \end{aligned} \tag{2}$$

where the factor

$$\chi = \frac{1}{2}\left(1-\frac{\Lambda_{44}^0}{\Lambda_{33}^0}\right)\left[\left(1+\frac{4\kappa_3\sin^2\theta\cos^2\theta}{\left(1-\frac{\Lambda_{44}^0}{\Lambda_{33}^0}\right)^2}+\frac{4\left(1-\frac{\Lambda_{44}^0}{\Lambda_{33}^0}+\kappa_1\right)\kappa_1\sin^4\theta}{\left(1-\frac{\Lambda_{44}^0}{\Lambda_{33}^0}\right)^2}\right)^{1/2}-1\right], \tag{3}$$

and κ_1, κ_2, and κ_3 are three stress-induced anisotropy coefficients given by[43]

$$\begin{aligned} \kappa_1 &= \frac{\Lambda_{11}^0-\Lambda_{33}^0}{2\Lambda_{33}^0}, \\ \kappa_2 &= \frac{\Lambda_{11}^0-\Lambda_{12}^0-2\Lambda_{44}^0}{4\Lambda_{44}^0} = \frac{\Lambda_{66}^0-\Lambda_{44}^0}{2\Lambda_{44}^0}, \text{ and} \\ \kappa_3 &= \frac{1}{2\Lambda_{33}^{0\,2}}\left[2\left(\Lambda_{13}^0+\Lambda_{44}^0\right)^2-\left(\Lambda_{33}^0-\Lambda_{44}^0\right)\times\left(\Lambda_{11}^0+\Lambda_{33}^0-2\Lambda_{44}^0\right)\right]. \end{aligned} \tag{4}$$

In Eqs. (2)–(4), $\boldsymbol{\Lambda}^0$ is a fourth-rank stress-dependent tensor consisting of ensemble averages of the second- and third-order single-crystal elastic constants of the grains. An example analytical expression for Λ_{33}^0 is given in the Appendix. Explicit forms for the other components are given elsewhere.[42] The phase velocities depend on the angle between the propagation direction and the direction of the uniaxial stress (θ or θ' for incident or scattered waves, respectively). Equation (2) takes advantage of the fact that the uniaxial stress results in a stress-induced transverse isotropy of $\boldsymbol{\Lambda}^0$

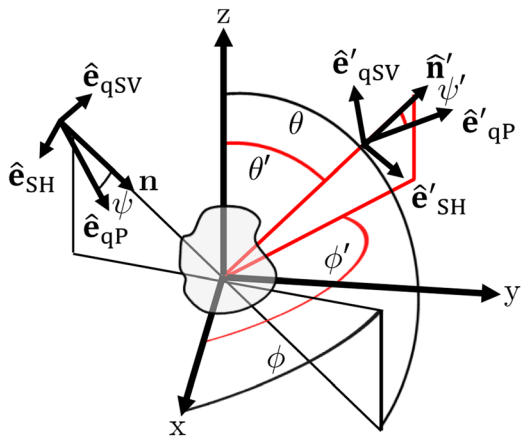

FIG. 1. (Color online) Coordinate system used to define the incoming wave vectors (unprimed variables) and scattered wave vectors (primed variables).

about the stress direction. Due to the anisotropy, Eq. (2) was easily written by extending Thomsen's formula for wave propagation in transversely isotropic materials where κ_1, κ_2, and κ_3 are the well-known Thomsen anisotropy parameters.[43]

The stress-induced anisotropy causes the wave displacement vectors to rotate within the plane containing the vectors $\hat{\mathbf{z}}$ and $\hat{\mathbf{n}}$ where σ_{33} is along the $\hat{\mathbf{z}}$ direction. The spherical coordinate system illustrated in Fig. 1 is used to define the scattering configuration. The vectors needed to define the propagation and displacement directions are given as

$$\begin{aligned}
\hat{\mathbf{n}} &= \hat{\mathbf{x}}\cos\phi\sin\theta + \hat{\mathbf{y}}\sin\phi\sin\theta + \hat{\mathbf{z}}\cos\theta,\\
\hat{\mathbf{e}}_{qP} &= \hat{\mathbf{x}}\cos\phi\sin[\theta+\psi(\theta)] + \hat{\mathbf{y}}\sin\phi\sin[\theta+\psi(\theta)]\\
&\quad + \hat{\mathbf{z}}\cos[\theta+\psi(\theta)],\\
\hat{\mathbf{e}}_{qSV} &= -\hat{\mathbf{x}}\cos\phi\cos[\theta+\psi(\theta)] - \hat{\mathbf{y}}\sin\phi\cos[\theta+\psi(\theta)]\\
&\quad + \hat{\mathbf{z}}\sin[\theta+\psi(\theta)], \text{ and}\\
\hat{\mathbf{e}}_{SH} &= \hat{\mathbf{x}}\sin\phi - \hat{\mathbf{y}}\cos\phi,
\end{aligned} \tag{5}$$

where $\psi(\theta)$ defines the stress-induced rotation of the qP and qSV wave modes and is defined as[44,45]

$$\psi(\theta) = -\frac{1}{2}\operatorname{atan}\left[\tan 2\theta \times \frac{H\cos^2\theta - \Lambda^0_{11} + \Lambda^0_{13} + 2\Lambda^0_{44}}{H\cos^2\theta + \left(-\Lambda^0_{11} + 2\Lambda^0_{13} + 3\Lambda^0_{44}\right)\sec 2\theta}\right], \tag{6}$$

with $H = \Lambda^0_{11} - 2\Lambda^0_{13} + \Lambda^0_{33} - 4\Lambda^0_{44}$. The rotation of the displacement directions is illustrated in Fig. 1. It is observed that $\psi = 0$ when no stress is present or when the propagation direction is parallel or perpendicular to the $\hat{\mathbf{z}}$ axis (the uniaxial stress direction).

Substitution of Eqs. (2)–(6) into Eq. (1) allows the stress-dependent scattering coefficients $\Omega^{I\to S}$ to be evaluated. The primed quantities related to the scattered wave in Eq. (1) require the use of the scattering angles θ', ϕ', and ψ' (Fig. 1) in Eqs. (2)–(6). Once these substitutions are performed, the stress-dependent scattering coefficients $\Omega^{I\to S}$ can be analyzed for different wave modes, propagation directions, propagation frequencies, grain sizes, and stress levels.

III. RESULTS AND DISCUSSION

In this section, the stress-dependence of the scattering of ultrasound from grains in a polycrystal is evaluated quantitatively. To achieve this end, the stress-dependent scattering coefficients are evaluated for a specific polycrystalline material (aluminum) and a uniaxial stress of magnitude σ_{33}, which acts along the z-direction. The first analysis given in Sec. III A considers the nine possible scattering coefficients: $\Omega^{qP\to qP}$, $\Omega^{qP\to qSV}$, $\Omega^{qP\to SH}$, $\Omega^{qSV\to qP}$, $\Omega^{qSVP\to qSV}$, $\Omega^{qSV\to SH}$, $\Omega^{SH\to qP}$, $\Omega^{SH\to qSV}$, $\Omega^{SH\to SH}$, which are simplified from Eq. (1) for a wave incident in the z-direction (parallel to the uniaxial stress σ_{33}) that scatters into all directions. The subsequent analysis, in Sec. III B, considers the incident waves to be normal to the z-direction or perpendicular to the uniaxial stress σ_{33}, which again scatters into any direction. Last, Secs. III C and III D consider backward and forward scattered waves, respectively, with each direction defined relative to the direction of the incident wave. Backscattering occurs when the scattering is into the direction opposite of the incident wave. Forward scattering defines the energy scattered in to the direction coincident with the incident wave. In Secs. III C and III D, the influence of grain size and frequency is considered also.

A. Wave incidence in the stress direction

Consider an incident wave propagating in the direction of the uniaxial stress, $\hat{\mathbf{n}} = -\hat{\mathbf{z}}$. For this case, the scattering coefficients are independent of the scattering angle ϕ' and are dependent on the scattering angle θ' only (in addition to the rotation angle ψ'). Using the definitions in Eqs. (2)–(6), the general form of the scattering coefficients can be obtained from Eq. (1) for all scattering mode types. For example, the three scattering coefficients for an incident qP wave are

$$\begin{aligned}
\Omega^{qP\to qP} = &\frac{v_{qP}^{-3}v_{qP}'^{-5}}{2\pi\rho^2}\frac{L^3}{\left[\omega^{-2}+L^2\left(v_{qP}^{-2}+v_{qP}'^{-2}+2v_{qP}^{-1}v_{qP}'^{-1}\cos\theta'\right)\right]^2}\\
&\times\left\{\Xi_{33}^{33}\cos^2\left(\theta'+\psi'\right)\cos^2\theta'\right.\\
&+\frac{1}{4}\Xi_{13}^{33}\left[\cos 2\psi' - \cos\left(4\theta'+2\psi'\right)\right]\\
&-\frac{1}{2}\Xi_{35}^{35}\left[\cos\left(4\theta'+2\psi'\right)-1\right]\\
&\left.+\Xi_{13}^{13}\left[\sin^2\left(\theta'+\psi'\right)\sin^2\theta'\right]\right\},
\end{aligned}$$

$$\Omega^{\mathrm{qP}\to\mathrm{qSV}} = \frac{v_{\mathrm{qP}}^{-3} v_{\mathrm{qSV}}'^{-5}}{2\pi\rho^2} \frac{L^3}{\left[\omega^{-2} + L^2\left(v_{\mathrm{qP}}^{-2} + v_{\mathrm{qSV}}'^{-2} + 2v_{\mathrm{qP}}^{-1} v_{\mathrm{qSV}}'^{-1}\cos\theta'\right)\right]^2} \left\{\Xi_{33}^{33}\sin^2(\theta'+\psi')\cos^2\theta' \right.$$
$$\left. -\frac{1}{4}\Xi_{13}^{33}\left[\cos 2\psi' - \cos(4\theta'+2\psi')\right] + \frac{1}{2}\Xi_{35}^{35}\left[\cos(4\theta'+2\psi')+1\right] + \Xi_{13}^{13}\left[\cos^2(\theta'+\psi')\sin^2\theta'\right]\right\},$$

$$\Omega^{\mathrm{qP}\to\mathrm{SH}} = \frac{v_{\mathrm{qP}}^{-3} v_{\mathrm{SH}}'^{-5}}{2\pi\rho^2} \frac{L^3\left(\Xi_{35}^{35}\cos^2\theta' + \Xi_{36}^{36}\sin^2\theta'\right)}{\left[\omega^{-2} + L^2\left(v_{\mathrm{qP}}^{-2} + v_{\mathrm{SH}}'^{-2} + 2v_{\mathrm{qP}}^{-1} v_{\mathrm{SH}}'^{-1}\cos\theta'\right)\right]^2}.$$

For an incident qSV wave,

$$\Omega^{\mathrm{qSV}\to\mathrm{qP}} = \frac{v_{\mathrm{qSV}}^{-3} v_{\mathrm{qP}}'^{-5}}{2\pi\rho^2} \frac{L^3}{\left[\omega^{-2} + L^2\left(v_{\mathrm{qSV}}^{-2} + v_{\mathrm{qP}}'^{-2} + 2v_{\mathrm{qSV}}^{-1} v_{\mathrm{qP}}'^{-1}\cos\theta'\right)\right]^2} \left\{\frac{1}{4}\Xi_{15}^{35}\left[\cos 2\psi' - \cos(2\psi'+4\theta')\right] \right.$$
$$\left. -\frac{1}{2}\Xi_{55}^{55}\left[\cos(2\psi'+4\theta')-1\right] + \Xi_{15}^{15}\sin^2(\psi'+\theta')\sin^2\theta' + \Xi_{35}^{35}\cos^2(\psi'+\theta')\cos^2\theta'\right\},$$

$$\Omega^{\mathrm{qSV}\to\mathrm{qSV}} = \frac{v_{\mathrm{qSV}}^{-3} v_{\mathrm{qSV}}'^{-5}}{2\pi\rho^2} \frac{L^3}{\left[\omega^{-2} + L^2\left(v_{\mathrm{qSV}}^{-2} + v_{\mathrm{qSV}}'^{-2} + 2v_{\mathrm{qSV}}^{-1} v_{\mathrm{qSV}}'^{-1}\cos\theta'\right)\right]^2} \left\{\frac{1}{2}\Xi_{55}^{55}\left[\cos(2\psi'+4\theta')+1\right] - \frac{1}{4}\Xi_{15}^{35}\left[\cos 2\psi' \right.\right.$$
$$\left.\left. -\cos(2\psi'+4\theta')\right] + \Xi_{15}^{15}\cos^2(\psi'+\theta')\sin^2\theta' + \Xi_{35}^{35}\sin^2(\psi'+\theta')\cos^2\theta'\right\},$$

$$\Omega^{\mathrm{qSV}\to\mathrm{SH}} = \frac{v_{\mathrm{qSV}}^{-3} v_{\mathrm{SH}}'^{-5}}{2\pi\rho^2} \frac{L^3\left(\Xi_{45}^{45}\cos^2\theta' + \Xi_{56}^{56}\sin^2\theta'\right)}{\left[\omega^{-2} + L^2\left(v_{\mathrm{qSV}}^{-2} + v_{\mathrm{SH}}'^{-2} + 2v_{\mathrm{qSV}}^{-1} v_{\mathrm{SH}}'^{-1}\cos\theta'\right)\right]^2},$$

while for an incident SH wave,

$$\Omega^{\mathrm{SH}\to\mathrm{qP}} = \frac{v_{\mathrm{SH}}^{-3} v_{\mathrm{qP}}'^{-5}}{2\pi\rho^2} \frac{L^3}{\left[\omega^{-2} + L^2\left(v_{\mathrm{SH}}^{-2} + v_{\mathrm{qP}}'^{-2} + 2v_{\mathrm{SH}}^{-1} v_{\mathrm{qP}}'^{-1}\cos\theta'\right)\right]^2} \left\{\frac{1}{4}\Xi_{14}^{34}\left[\cos(2\psi') - \cos(2\psi'+4\theta')\right] \right.$$
$$\left. -\frac{1}{2}\Xi_{45}^{45}\left(\cos(2\psi'+4\theta')-1\right) + \Xi_{14}^{14}\sin^2(\psi'+\theta')\sin^2\theta' + \Xi_{35}^{35}\cos^2(\psi'+\theta')\cos^2\theta'\right\},$$

$$\Omega^{\mathrm{SH}\to\mathrm{qSV}} = \frac{v_{\mathrm{SH}}^{-3} v_{\mathrm{qSV}}'^{-5}}{2\pi\rho^2} \frac{L^3}{\left[\omega^{-2} + L^2\left(v_{\mathrm{SH}}^{-2} + v_{\mathrm{qSV}}'^{-2} + 2v_{\mathrm{SH}}^{-1} v_{\mathrm{qSV}}'^{-1}\cos\theta'\right)\right]^2} \left\{\frac{1}{2}\Xi_{45}^{45}\left[\cos(2\psi'+4\theta')+1\right] \right.$$
$$\left. -\frac{1}{4}\Xi_{14}^{34}\left[\cos(2\psi') - \cos(2\psi'+4\theta')\right] + \Xi_{14}^{14}\cos^2(\psi'+\theta')\sin^2\theta' + \Xi_{35}^{35}\sin^2(\psi'+\theta')\cos^2\theta'\right\}, \quad \text{and}$$

$$\Omega^{\mathrm{SH}\to\mathrm{SH}} = \frac{v_{\mathrm{SH}}^{-3} v_{\mathrm{SH}}'^{-5}}{2\pi\rho^2} \frac{L^3\left(\Xi_{55}^{55}\cos^2\theta' + \Xi_{56}^{56}\sin^2\theta'\right)}{\left[\omega^{-2} + L^2\left(v_{\mathrm{SH}}^{-2} + v_{\mathrm{SH}}'^{-2} + 2v_{\mathrm{SH}}^{-1} v_{\mathrm{SH}}'^{-1}\cos\theta'\right)\right]^2}. \tag{7}$$

A quantitative evaluation of the nine stress-dependent scattering coefficients is shown in Fig. 2 for polycrystalline aluminum. The scattering coefficients were evaluated using the single-crystal elastic constants of aluminum given in Table II and a density of 2700 kg/m^3. In addition, a grain radius of $L = 15\,\mu$m and a frequency of $f = 10$ MHz were chosen for the analysis, which represent realistic values. The scattering coefficients are plotted for different levels of uniaxial stress, $\sigma_{33} = -500$ MPa, -250 MPa, 0 MPa, 250 MPa, and 500 MPa, for which a negative value indicates a compressive load. Each coefficient is plotted against the scattering angle θ'. Thus, the incident wave is scattered into the opposite direction when $\theta' = 0$, the forward direction when $\theta' = \pi$, and perpendicular to the stress direction when $\theta' = \pi/2$. The scattering coefficients are shown to be highly stress dependent. For example, $\Omega^{\mathrm{qP}\to\mathrm{qP}}$ for the backscattered wave ($\theta' = 0$) changes by about 38% when increasing the compressive stress from $\sigma_{33} = 0$ MPa to $\sigma_{33} = -500$ MPa.

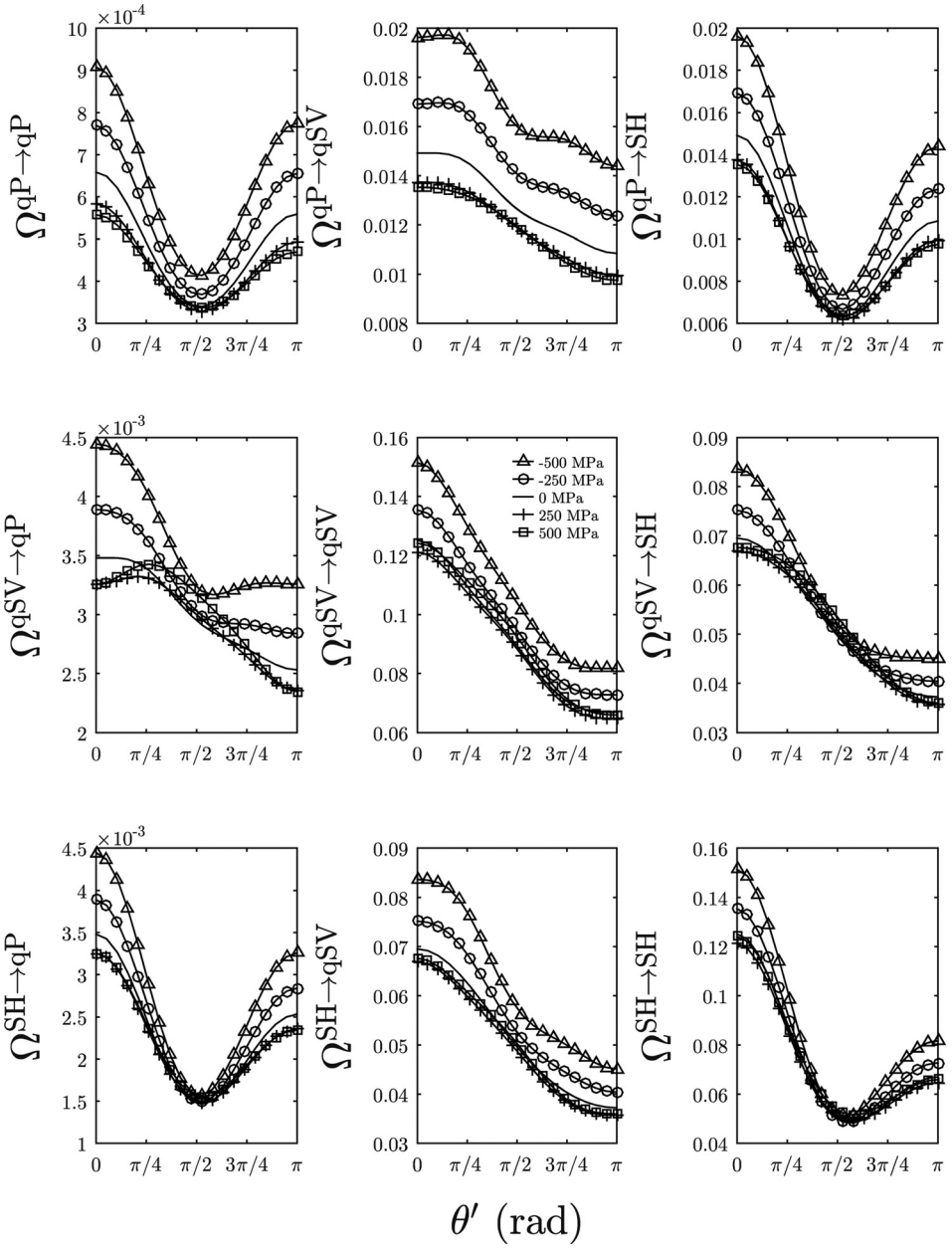

FIG. 2. Stress-dependent scattering coefficients Ω (in units of m^{-1}) for an incident wave in the direction of uniaxial stress σ_{33} that scatters in the direction θ' for polycrystalline aluminum, $f = 10$ MHz, and $L = 15\,\mu$m. The following symbols represent the values of uniaxial stress: -500 MPa (△), -250 MPa (o), 0 MPa (−), 250 MPa (+), and 500 MPa (□).

In comparison, the phase velocity of a qP wave propagating in the direction of uniaxial stress changes by 2% for the same compressional stress range.[26]

The stress-dependence is also shown to be highly nonlinear. For the scattering coefficient illustrated in Fig. 1, changes in the compressive stress have a stronger influence on the scattering coefficients than an equivalent change in tension. Additionally, the changes in the scattering coefficients are typically greater for a tensile stress that increases from 0 to 250 MPa than an increase from 250 to 500 MPa. The nonlinear stress dependence in the scattering coefficients is a result of the components of the covariance tensor $\boldsymbol{\Xi}$ being quadratic in stress.[26] Conversely, it was shown that the components of $\boldsymbol{\Xi}$ for iron behave linearly with the uniaxial stress, which would likely cause a linear stress-dependence in the scattering coefficients.[26]

The sensitivity of the scattering coefficients is highly dependent on the propagation or scattering directions with respect to the direction of stress. In Sec. III B, the incident wave will be perpendicular or normal to the uniaxial stress direction.

B. Wave incident normal to the stress direction

Next, the incident wave is considered to propagate in a direction that is perpendicular to the uniaxial stress, i.e., $\theta = \pi/2$ and $\hat{\mathbf{n}} \cdot \hat{\mathbf{z}} = 0$ from Fig. 1. In this case, the scattering coefficients are dependent on the incident angle ϕ and the two scattering angles θ' and ϕ'. For brevity, explicit forms of these scattering coefficients are not given here, but can be found in detail elsewhere.[26]

In order to evaluate Ω quantitatively for this configuration, it is assumed that the mean grain radius and wave frequency are, again, $L = 15\,\mu$m and $f = 10$ MHz. The azimuthal angle of the incident wave is set to $\phi = \pi$ so that $\hat{\mathbf{n}} = -\hat{\mathbf{x}}$ in Fig. 1. Because of the dependence of Ω on the

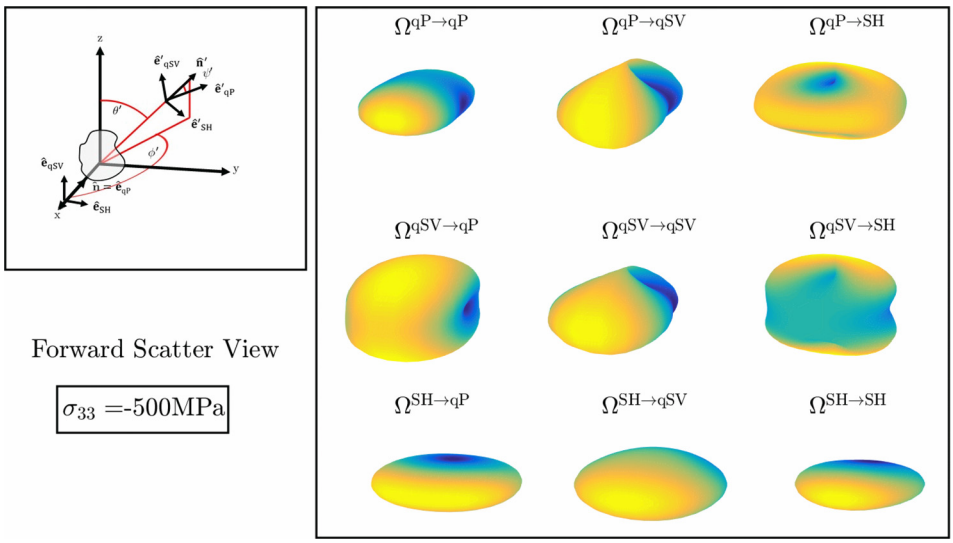

FIG. 3. (Color online) Stress-dependent scattering coefficients for aluminum. The incident wave is normal to the direction of uniaxial stress σ_{33} and scatters into the directions θ' and ϕ'. The illustration shows the forward scattering view.

two scattering angles θ' and ϕ', three-dimensional scattering surfaces were generated from each scattering mode type for different values of stress. Figures 3 and 4 illustrate the forward scattering and backscattering views of these surfaces for a 500 MPa compressive stress, respectively. Supplementary online resources provide animated versions of Figs. 3 and 4, which show the scattering amplitudes for values of uniaxial stress between − 500 and 500 MPa.[46] The forward scattering view in Fig. 3 illustrates the waves that have scattered forward into the $-\hat{\mathbf{x}}$-direction. This view is what an observer would see when they are viewing the x-y plane looking into the $+\hat{\mathbf{x}}$-direction. For the scattering coefficient $\Omega^{qP\to qP}$ the strongest forward scattering amplitudes are in the direction of the incident wave. However, other scattering mode types show that the maximum forward scattering amplitude is along other directions. Figure 4 illustrates the backscattered view. In this case, the observer is viewing the x-y plane into the $-\hat{\mathbf{x}}$-direction. In other words, the backscattered view in Fig. 4 is observing behind the surfaces illustrated in Fig. 3.

The stress-dependence of these scattering coefficients can be observed by viewing the animated versions of Figs. 3 and 4. The change in shape and color of the surfaces are a result of the change in uniaxial stress σ_{33}. These animations indicate the stress-dependence for the different possible scattering directions for each wave mode. For example, the amplitude of $\Omega^{qP\to qP}$ for backscattering into the $+\hat{\mathbf{x}}$-direction shown in Fig. 4 changes in magnitude from 5.12×10^{-4} to $6.73\times10^{-4}\,\mathrm{m}^{-1}$ or 31.4% as the uniaxial stress changes from −500 MPa compression to 500 MPa tension. However, this scattering coefficient for an incident wave that scatters into the stress direction or $-\hat{\mathbf{z}}$-direction decreases from 3.94×10^{-4} to $3.56\times10^{-4}\,\mathrm{m}^{-1}$ or −9.7% over this range.

The configurations considered in Secs. III A and III B apply to experimental pitch/catch configurations of transducers in which one transducer is used as a source and the other receives the scattered waves. A special case exists when the source and receiving transducer are at the same location in space. For this case, the experimental configuration is referred to as a pulse-echo backscatter because the same transducer is used to both transmit the incident wave and receive the scattered waves that have scattered into the opposite direction back to the transducer. Section III C considers the stress-dependence on the backscatter coefficients.

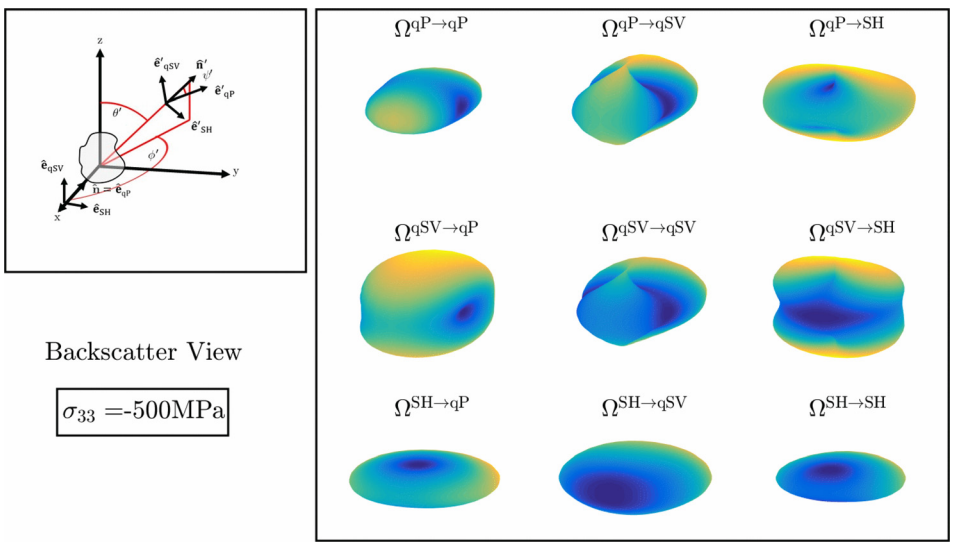

FIG. 4. (Color online) Stress-dependent scattering coefficients for aluminum. The incident wave is normal to the direction of uniaxial stress σ_{33} and scatters into the directions θ' and ϕ'. The illustration shows the backscattering view.

C. Backscattered wave

For a backscatter configuration, the scattered wave field received is the component of the scattering that has scattered into the direction opposite of the incident wave. Thus, the incident wave direction can be defined using the angles θ and ϕ, while the scattered directions are $\theta' = \theta - \pi$ and $\phi' = \phi$. For these angles, the inner product between the incident and scattered wave directions is $\hat{n}_p \hat{n}'_p = -1$. Explicit forms of the backscatter coefficients can be given for the special directions where the backscattering occurs in a direction parallel or perpendicular to the direction of the uniaxial stress. The backscatter coefficients for scattering in the direction of the uniaxial stress are

$$
\begin{aligned}
&\Omega^{\mathrm{qP}\parallel\to\mathrm{qP}\parallel} = \frac{v_{\mathrm{qP}\parallel}^{-8}}{2\pi\rho^2} L^3\, \Xi_{33}^{33}\left(\omega^{-2} + 4L^2 v_{\mathrm{qP}\parallel}^{-2}\right)^{-2},\\
&\Omega^{\mathrm{qP}\parallel\to\mathrm{qSV}\parallel} = \frac{v_{\mathrm{qP}\parallel}^{-3} v_{\mathrm{qSV}\parallel}^{-5}}{2\pi\rho^2} L^3\, \Xi_{35}^{35}\left[\omega^{-2} + L^2\left(v_{\mathrm{qP}\parallel}^{-1} + v_{\mathrm{qSV}\parallel}^{-1}\right)^2\right]^{-2},\\
&\Omega^{\mathrm{qP}\parallel\to\mathrm{SH}\parallel} = \Omega^{\mathrm{qP}\parallel\to\mathrm{qSV}\parallel}, \quad \Omega^{\mathrm{qSV}\parallel\to\mathrm{qP}\parallel} = \frac{v_{\mathrm{qSV}\parallel}^2}{v_{\mathrm{qP}\parallel}^2}\Omega^{\mathrm{qP}\parallel\to\mathrm{qSV}\parallel},\\
&\Omega^{\mathrm{qSV}\parallel\to\mathrm{qSV}\parallel} = \frac{v_{\mathrm{qSV}\parallel}^{-8}}{2\pi\rho^2}\frac{L^3\,\Xi_{55}^{55}}{\left(\omega^{-2} + 4L^2 v_{\mathrm{qSV}\parallel}^{-2}\right)^2}, \quad \Omega^{\mathrm{qSV}\parallel\to\mathrm{SH}\parallel} = \frac{v_{\mathrm{qSV}\parallel}^{-8}}{2\pi\rho^2}\frac{L^3\,\Xi_{45}^{45}}{\left(\omega^{-2} + 4L^2 v_{\mathrm{qSV}\parallel}^{-2}\right)^2},\\
&\Omega^{\mathrm{SH}\parallel\to\mathrm{qP}\parallel} = \Omega^{\mathrm{qSV}\parallel\to\mathrm{qP}\parallel}, \quad \Omega^{\mathrm{SH}\parallel\to\mathrm{qSV}\parallel} = \Omega^{\mathrm{qSV}\parallel\to\mathrm{SH}\parallel}, \quad \text{and} \quad \Omega^{\mathrm{SH}\parallel\to\mathrm{SH}\parallel} = \Omega^{\mathrm{qSV}\parallel\to\mathrm{qSV}\parallel},
\end{aligned}
\tag{8}
$$

where the symbol $\parallel$ was added to the superscripts in order to denote that the scattering occurs parallel to the uniaxial stress. The symmetry caused by the uniaxial stress causes in the incident and scattered shear wave modes to be degenerate. Thus, several of the scattering coefficients are equal. The scattering coefficients for scattering that occurs perpendicular to the uniaxial stress are given as

$$
\begin{aligned}
&\Omega^{\mathrm{qP}\perp\to\mathrm{qP}\perp} = \frac{v_{\mathrm{qP}\perp}^{-8}}{2\pi\rho^2} L^3\, \Xi_{11}^{11}\left(\omega^{-2} + 4L^2 v_{\mathrm{qP}\perp}^{-2}\right)^{-2},\\
&\Omega^{\mathrm{qP}\perp\to\mathrm{qSV}\perp} = \frac{v_{\mathrm{qP}\perp}^{-3} v_{\mathrm{qSV}\perp}^{-5}}{2\pi\rho^2} L^3\, \Xi_{15}^{15}\left[\omega^{-2} + L^2\left(v_{\mathrm{qP}\perp}^{-1} + v_{\mathrm{qSV}\perp}^{-1}\right)^2\right]^{-2},\\
&\Omega^{\mathrm{qP}\perp\to\mathrm{SH}\perp} = \frac{v_{\mathrm{qP}\perp}^{-3} v_{\mathrm{SH}\perp}^{-5}}{2\pi\rho^2} L^3\, \Xi_{16}^{16}\left[\omega^{-2} + L^2\left(v_{\mathrm{qP}\perp}^{-1} + v_{\mathrm{SH}\perp}^{-1}\right)^2\right]^{-2},\\
&\Omega^{\mathrm{qSV}\perp\to\mathrm{qP}\perp} = \frac{v_{\mathrm{qSV}\perp}^2}{v_{\mathrm{qP}\perp}^2}\Omega^{\mathrm{qP}\perp\to\mathrm{qSV}\perp}, \quad \Omega^{\mathrm{qSV}\perp\to\mathrm{qSV}\perp} = \frac{v_{\mathrm{qSV}\perp}^{-8}}{2\pi\rho^2} L^3\, \Xi_{55}^{55}\left(\omega^{-2} + 4L^2 v_{\mathrm{qSV}\perp}^{-2}\right)^{-2},\\
&\Omega^{\mathrm{qSV}\perp\to\mathrm{SH}\perp} = \frac{v_{\mathrm{qSV}\perp}^{-3} v_{\mathrm{SH}\perp}^{-5}}{2\pi\rho^2} L^3\, \Xi_{56}^{56}\left[\omega^{-2} + L^2\left(v_{\mathrm{qSV}\perp}^{-1} + v_{\mathrm{SH}\perp}^{-1}\right)^2\right]^{-2},\\
&\Omega^{\mathrm{SH}\perp\to\mathrm{qP}\perp} = \frac{v_{\mathrm{SH}\perp}^2}{v_{\mathrm{qP}\perp}^2}\Omega^{\mathrm{qP}\perp\to\mathrm{SH}\perp}, \quad \Omega^{\mathrm{SH}\perp\to\mathrm{qSV}\perp} = \frac{v_{\mathrm{SH}\perp}^2}{v_{\mathrm{qSV}\perp}^2}\Omega^{\mathrm{qSV}\perp\to\mathrm{SH}\perp}, \quad \text{and}\\
&\Omega^{\mathrm{SH}\perp\to\mathrm{SH}\perp} = \frac{v_{\mathrm{SH}\perp}^{-8}}{2\pi\rho^2} L^3\, \Xi_{66}^{66}\left(\omega^{-2} + 4L^2 v_{\mathrm{SH}\perp}^{-2}\right)^{-2},
\end{aligned}
\tag{9}
$$

where the symbol $\perp$ indicates this case.

The backscattered response is symmetric about the direction of uniaxial stress for the propagation and displacement directions defined in Fig. 1. Thus, the backscatter coefficients can be evaluated as a function of the incident angle θ and independent of the azimuthal angles ϕ or ϕ'. Figure 5 illustrates the stress-dependence of the backscattered energy as a function of angle θ. The frequency and grain size are assumed to be $f = 10$ MHz and $L = 15$ μm, respectively. The expressions given in Eq. (8) are represented by the data points along $\theta = 0$, which represent the backscatter in the direction of the uniaxial stress. The data points along $\theta = \pi/2$ represent backscatter perpendicular or normal to the direction of uniaxial stress, which are given by the expressions in Eq. (9). The stress-dependence of the scattering coefficients when an SH wave mode is involved is shown to be large for propagation directions perpendicular to the uniaxial stress. However, most backscattered waves are shown

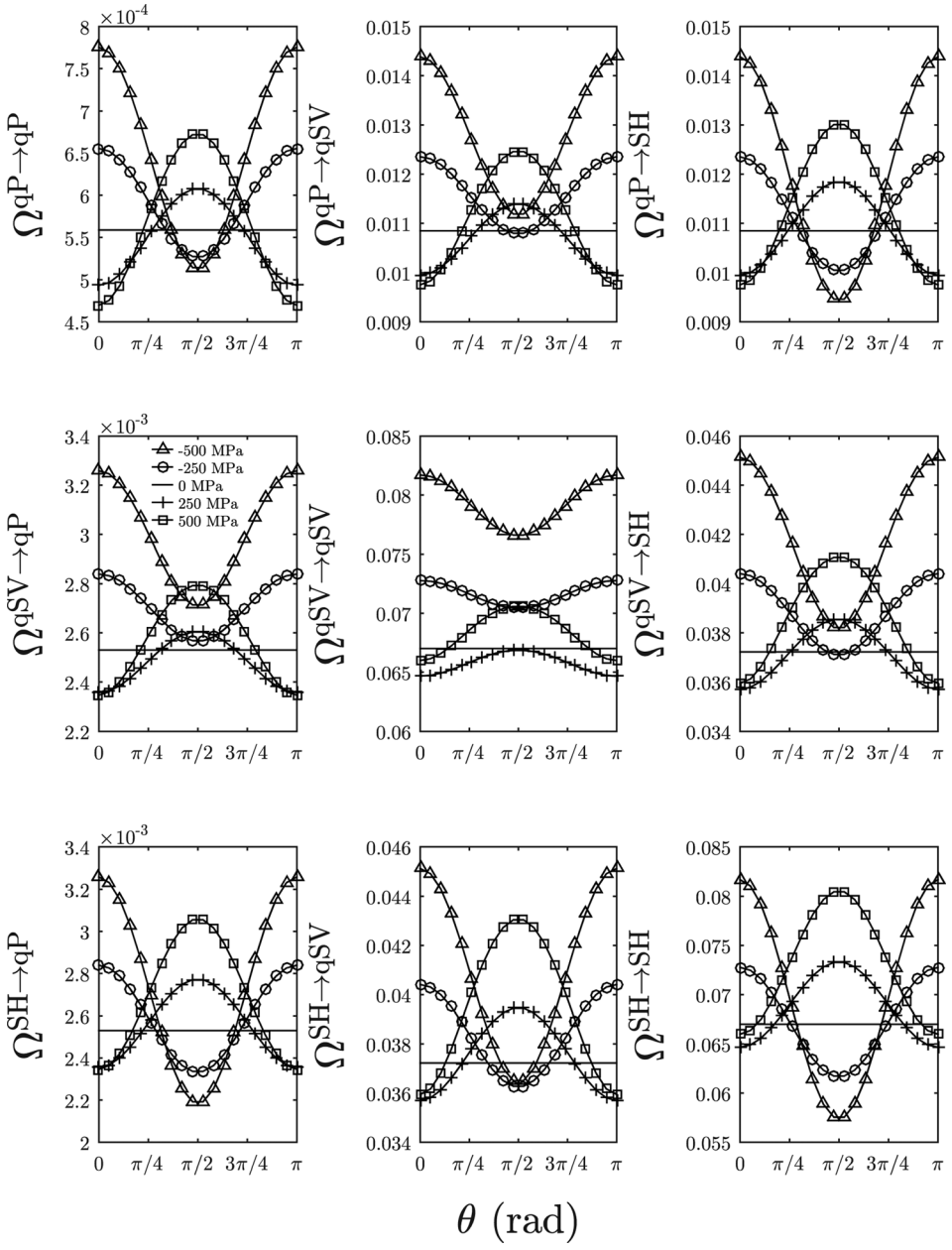

FIG. 5. Stress-dependent scattering coefficients Ω (in units of m^{-1}) for an incident wave in the direction θ from the direction of uniaxial stress σ_{33} that backscatters in the opposite direction $\theta' = \theta - \pi$ for polycrystalline aluminum, $f = 10$ MHz, and $L = 15\ \mu$m. The following symbols represent the values of uniaxial stress: -500 MPa ($\triangle$), -250 MPa (o), 0 MPa ($-$), 250 MPa ($+$), and 500 MPa ($\square$).

to have the greatest stress-dependence when the propagation directions are parallel to the direction of uniaxial stress. This trend is especially true for longitudinal waves for which $\Omega^{qP\|\to qP\|}$ increases by 38.8% for increasing compression from 0 to -500 MPa, while $\Omega^{qP\perp\to qP\perp}$ decreases by 8.3% over this same range. This example demonstrates the strong influence of the stress-induced anisotropy on the scattered waves, whereas $\Omega^{qP\|\to qP\|} = \Omega^{qP\perp\to qP\perp}$ when the material is stress-free and statistically isotropic.

1. Influence of grain size and frequency

The previous evaluation of the scattering coefficients assumed the grain radius and frequency to be 15 μm and 10 MHz, respectively. In this section, the stress-dependence of the scattering coefficients are evaluated for different grain sizes and ultrasonic frequencies. Figure 6 illustrates the stress-dependent scattering coefficients for an incident and backscattered wave along the uniaxial stress direction. Each stress-dependent scattering coefficient $\Omega^{qP\|\to qP\|}(\sigma_{33})$ is normalized by its zero stress value,

$$\Omega_0^{qP\|\to qP\|} \equiv \frac{\Omega^{qP\|\to qP\|}(\sigma_{33})}{\Omega^{qP\|\to qP\|}(\sigma_{33}=0)}. \tag{10}$$

The frequency of the input wave is chosen to be 10 MHz in order to investigate how the grain size influences the stress sensitivity of $\Omega_0^{qP\|\to qP\|}$. Conversely, the grain radius is assumed to be $L = 15\ \mu$m when observing the frequency dependence. For this scattering coefficient, the sensitivity to σ_{33} is magnified at larger grain sizes and frequencies. The increase begins for values of f and L that cause the scattering to exceed the Rayleigh scattering limit. At high frequencies or grain sizes, $\Omega_0^{qP\|\to qP\|}$ increases by 50% for increasing compression from 0 to -500 MPa. Increasing tension from 0 to 500 MPa results in a decrease of the scattering coefficient by 22.5%. An evaluation of the frequency and grain size influence for other scattering modes is available elsewhere.[26]

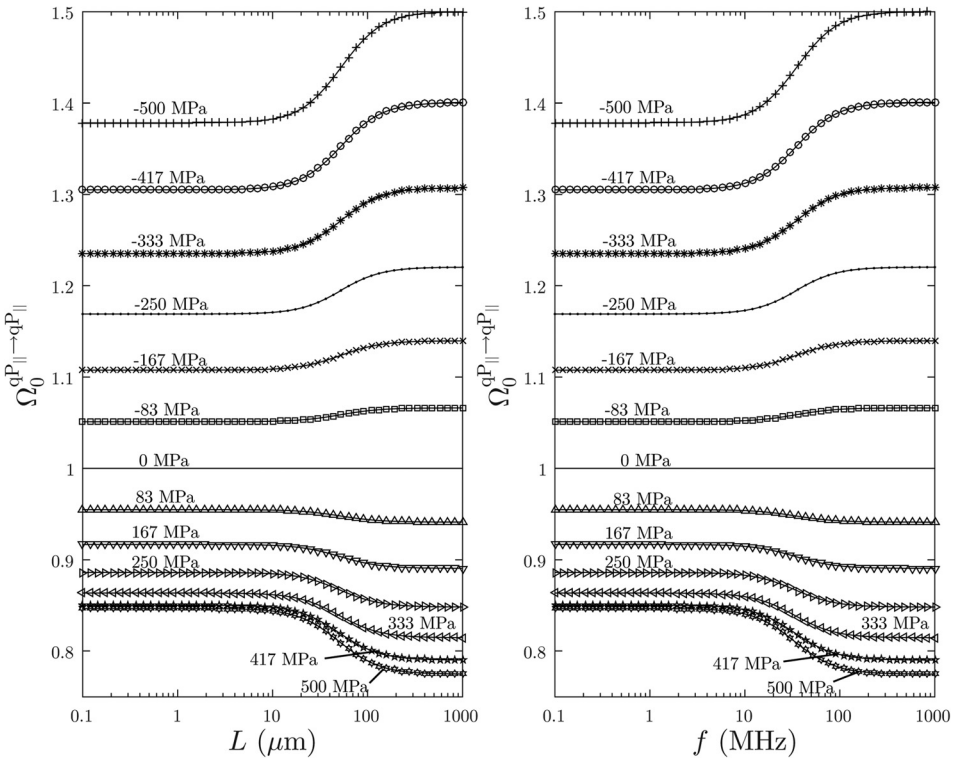

FIG. 6. The influence of grain radius (L) and frequency (f) on the stress-dependence of the qP backscatter coefficient of aluminum when the incident and scattered wave directions are parallel to the direction of uniaxial stress σ_{33}.

D. Forward scattered wave

A forward scattered wave is produced when observing the scattered response in the direction of the incident wave. In an experimental setting, the response of the forward scattered wave is captured by using a receiving transducer that faces or is in line with the source transducer while the sample is situated equidistance between the transducers. Scattering coefficients for the forward scattering configuration are obtained with the conditions, $\theta = \theta'$, $\phi = \phi'$, and $\hat{n}_p \hat{n}'_p = 1$. The simplest forms of the stress-dependent scattering coefficients are observed when the propagation direction is either parallel or perpendicular to the direction of uniaxial stress. For the parallel case, the nine scattering coefficients are given as

$$\Omega^{qP\parallel\to qP\parallel} = \frac{v_{qP\parallel}^{-8}\omega^4}{2\pi\rho^2} L^3\, \Xi_{33}^{33}, \quad \Omega^{qP\parallel\to qSV\parallel} = \frac{v_{qP\parallel}^{-3} v_{qSV\parallel}^{-5}}{2\pi\rho^2} L^3\, \Xi_{35}^{35} \left[\omega^{-2} + L^2\left(v_{qP\parallel}^{-1} - v_{qSV\parallel}^{-1}\right)^2\right]^{-2},$$

$$\Omega^{qP\parallel\to SH\parallel} = \Omega^{qP\parallel\to qSV\parallel}, \quad \Omega^{qSV\parallel\to qP\parallel} = \frac{v_{qSV\parallel}^2}{v_{qP\parallel}^2}\Omega^{qP\parallel\to qSV\parallel}, \quad \Omega^{qSV\parallel\to qSV\parallel} = \frac{v_{qSV\parallel}^{-8}\omega^4}{2\pi\rho^2} L^3\, \Xi_{55}^{55}$$

$$\Omega^{qSV\parallel\to SH\parallel} = \frac{v_{qSV\parallel}^{-8}\omega^4}{2\pi\rho^2} L^3\, \Xi_{45}^{45}, \quad \Omega^{SH\parallel\to qP\parallel} = \Omega^{qSV\parallel\to qP\parallel}, \quad \Omega^{SH\parallel\to qSV\parallel} = \Omega^{qSV\parallel\to SH\parallel}, \quad \text{and}$$

$$\Omega^{SH\parallel\to SH\parallel} = \Omega^{qSV\parallel\to qSV\parallel}. \tag{11}$$

For this case, $v_{qSV} = v'_{qSV} = v_{SH} = v'_{SH}$ because of the symmetry about the direction of stress. The stress-dependence of the scattering coefficients in Eq. (11) is illustrated in Fig. 2 for the case when $\theta' = \pi$. When the propagation directions are perpendicular to the uniaxial stress, the scattering coefficients are found to be

$$\Omega^{qP\perp\to qP\perp} = \frac{v_{qP\perp}^{-8}\omega^4}{2\pi\rho^2} L^3\, \Xi_{11}^{11},$$

$$\Omega^{qP\perp\to qSV\perp} = \frac{v_{qP\perp}^{-3} v_{qSV\perp}^{-5}}{2\pi\rho^2} L^3\, \Xi_{15}^{15} \left[\omega^{-2} + L^2\left(v_{qP\perp}^{-1} - v_{qSV\perp}^{-1}\right)^2\right]^{-2},$$

$$\Omega^{qP\perp\to SH\perp} = \frac{v_{qP\perp}^{-3} v_{SH\perp}^{-5}}{2\pi\rho^2} L^3\, \Xi_{16}^{16} \left[\omega^{-2} + L^2\left(v_{qP\perp}^{-1} - v_{SH\perp}^{-1}\right)^2\right]^{-2},$$

$$\Omega^{qSV\perp\to qP\perp} = \frac{v_{qSV\perp}^2}{v_{qP\perp}^2}\Omega^{qP\perp\to qSV\perp}, \quad \Omega^{qSV\perp\to qSV\perp} = \frac{v_{qSV\perp}^{-8}\omega^4}{2\pi\rho^2} L^3\, \Xi_{55}^{55},$$

$$\Omega^{\mathrm{qSV}\perp\to\mathrm{SH}\perp} = \frac{v_{\mathrm{qSV}\perp}^{-3} v_{\mathrm{SH}\perp}^{-5}}{2\pi\rho^2} L^3 \, \Xi_{56}^{56} \left[\omega^{-2} + L^2 \left(v_{\mathrm{qSV}\perp}^{-1} - v_{\mathrm{SH}\perp}^{-1}\right)^2\right]^{-2},$$

$$\Omega^{\mathrm{SH}\perp\to\mathrm{qP}\perp} = \frac{v_{\mathrm{SH}\perp}^2}{v_{\mathrm{qP}\perp}^2} \Omega^{\mathrm{qP}\perp\to\mathrm{SH}\perp}, \quad \Omega^{\mathrm{SH}\perp\to\mathrm{qSV}\perp} = \frac{v_{\mathrm{SH}\perp}^2}{v_{\mathrm{qSV}\perp}^2} \Omega^{\mathrm{qSV}\perp\to\mathrm{SH}\perp}, \quad \text{and}$$

$$\Omega^{\mathrm{SH}\perp\to\mathrm{SH}\perp} = \frac{v_{\mathrm{SH}\perp}^{-8} \omega^4}{2\pi\rho^2} L^3 \, \Xi_{66}^{66}. \tag{12}$$

The stress-dependence of these coefficients is shown in the animation that accompanies Fig. 3. For a forward scattered wave with the same phase velocity as the incident wave, $L^2(v^{-2} + v\prime^{-2} - 2v^{-1}v\prime^{-1}\hat{n}_p\hat{n}'_p) = 0$, which simplifies the denominator of Eq. (1). With this simplification, certain ratios of scattering coefficients from Eqs. (11) and (12) are independent of the frequency and grain dimensions. The ratios of the possible longitudinal and shear scattering coefficients reduce to

$$\frac{\Omega^{\mathrm{qP}\parallel\to\mathrm{qP}\parallel}}{\Omega^{\mathrm{qP}\perp\to\mathrm{qP}\perp}} = \left(\frac{v_{\mathrm{qP}\perp}}{v_{\mathrm{qP}\parallel}}\right)^8 \frac{\Xi_{33}^{33}}{\Xi_{11}^{11}},$$

$$\frac{\Omega^{\mathrm{qSV}\parallel\to\mathrm{qSV}\parallel}}{\Omega^{\mathrm{qSV}\perp\to\mathrm{qSV}\perp}} = \left(\frac{v_{\mathrm{qSV}\perp}}{v_{\mathrm{qSV}\parallel}}\right)^8, \quad \text{and}$$

$$\frac{\Omega^{\mathrm{SH}\parallel\to\mathrm{SH}\parallel}}{\Omega^{\mathrm{SH}\perp\to\mathrm{SH}\perp}} = \left(\frac{v_{\mathrm{SH}\perp}}{v_{\mathrm{SH}\parallel}}\right)^8 \frac{\Xi_{55}^{55}}{\Xi_{66}^{66}}. \tag{13}$$

The ratios of the qP and SH coefficients are functions of the acoustoelastic phase velocities and certain components of the covariance tensor. For the ratio involving the qSV modes, the response is governed only by the eighth-power of the ratio of phase velocities of the respective waves. Figure 7 illustrates how these ratios change as a function of uniaxial stress. An increase in uniaxial compression from 0 to −500 MPa results in an increase of 50.2%, 40.3%, and 7.8% for the qP, SH, and qSV ratios, respectively. Uniaxial tension highlights the quadratic nature of the ratios of scattering coefficients for which the stress-dependence is noticeably smaller than compression. The stress-dependence in Ξ is the cause of the greater sensitivity for the qP and SH ratios. Even though the qP and SH ratios are more sensitive to the uniaxial stress, the qSV ratio will only deviate from unity when stresses are present in the material. This result stems from the fact that differences between $v_{\mathrm{qSV}\perp}$ and $v_{\mathrm{qSV}\parallel}$ exist only because stresses are present rather than elastic anisotropy. This outcome is an extension of the stress-induced shear-wave birefringence observed in acoustoelastic phase velocities.

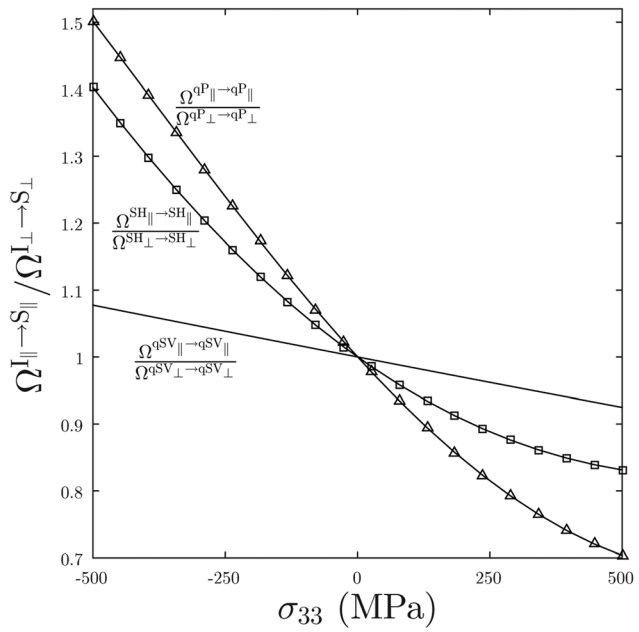

FIG. 7. Ratios between the forward scattering coefficients of aluminum for a wave propagating parallel and normal to the direction of uniaxial stress σ_{33}, respectively.

IV. CONCLUDING REMARKS

Equation (1) defines $\Omega^{\mathrm{I}\to\mathrm{S}}$, which is the differential scattering cross-section for scattering of ultrasound from grains in a stressed polycrystalline material. It represents the scattered energy into a direction that has been lost out of the incident coherently propagating wave due to scattering at grain boundaries. The introduction of the stress-dependence into $\Omega^{\mathrm{I}\to\mathrm{S}}$ was achieved by utilizing the stress-dependent elastic moduli of the polycrystal.[22] As was shown in Kube *et al.*,[42] the same stress-dependent elastic moduli can be used to model acoustoelasticity or the phase velocity dependence on the stress state of the polycrystalline material. Thus, the same physical mechanism that leads to stress-dependent phase velocities causes the scattering from grain boundaries to be influenced by material stresses. In fact, the present model predicts that grain scattering is much more sensitive to a uniaxial stress than the sensitivity of the phase velocity over the same stress range. This finding was demonstrated, for aluminum, in Sec. III A for a backscattered longitudinal wave in uniaxially stressed aluminum. This backscattering amplitude was predicted to change by 38% for an increase in uniaxial compression from 0 to −500 MPa. Over the same stress range, the value of the phase velocity for a longitudinal wave propagating in the direction of uniaxial stress changes by around 2%. The sensitivity improvement observed for scattering supports the potential of developing scattering based methods for stress measurement and monitoring applications. Additional results for both aluminum and iron can be located elsewhere.[26]

If $\Omega^{\mathrm{I}\to\mathrm{S}}$ is the loss of energy from the incident wave into a given direction due to scattering, the total energy removed from the incident wave can be considered as an integration of $\Omega^{\mathrm{I}\to\mathrm{S}}$ over all scattering directions. As shown by Weaver,

this integration over the scattering cross-sections is intimately related to the scattering contribution of the attenuation coefficient.[47] Thus, the influence of the stress-dependent scattering can be used to examine the influence of stress on attenuation coefficients in polycrystalline materials. Ogi *et al.*[18] and Hirao *et al.*[13] attributed the stress-dependence of the measured attenuation to absorption of energy due to changes in dislocation behavior during loading. Here, it has been shown that the stress-dependence of the grain scattering and the dislocation absorption may have competing influences on the measured attenuation coefficient. However, the measurement of the scattered response using previously described methods[24,25,48] are believed to be weakly influenced by dislocations. Thus, unlike attenuation measurement or phase velocity measurements,[13,18] the stress influence on the direct measurement of the scattered response is not coupled with stress-dependent dislocation influence.

Section III presented example results of the stress-influence on $\Omega^{I\to S}$ for a variety of scattering configurations. A scattering configuration consists mainly of two factors; the mode types of the incident and scattered waves and the direction of propagation of the incident and scattered wave with respect to the direction of stresses. Both the incident and scattered waves can be one of the three mode types qP, qSV, or SH, which results in nine possible configurations. Combinations of scattering measurements could be used to solve for unknown variables such as the average grain dimensions or to generate a desired measurement redundancy. Thus, the results given in Sec. III can be used as a guide for designing the optimal configuration of source and receiving transducers. Furthermore, Sec. III D considered the influence of stress on forward scattered waves. It was shown that certain ratios of forward scattered waves with different incident directions with respect to a uniaxial stress are independent of the mean grain dimensions. These ratios were shown to be intimately related to the traditional acoustoelastic effect where the ratios simplified to quotients containing eighth powers of the phase velocities. The ratio of the qSV forward scattering coefficients can deviate from unity only when a change of stress is present.

Some challenges will need to be overcome before using scattering-based techniques for stress measurements. Surface roughness, ultrasonic system variability, surface access constraints, etc., are a few prohibiting issues. Additionally, the present analysis has not included the possibility that the unstressed state of the material possessed elastic anisotropy or texture, which results from manufacturing processes. Thus, the scattered response will have competing effects of texture and stress for many polycrystalline materials. Texture can be accounted for in the present model by including a weighting factor on the ensemble averaged stress-dependent elastic constants. For stress-free materials, Yang and Rokhlin[49] and Li *et al.*[50] recently considered the texture effects on ultrasonic scattering. Certain scattering configurations could be shown to be independent of either stress or texture. Many of the configurations considered in Sec. III were weakly dependent on the stress. These configurations could be used to quantify texture while other configurations that are more sensitive to stresses could be used to measure the stress. Alternatively, a scattering based technique could be used in conjunction with other techniques such as phase velocity measurements in order to garner stress/texture information.

APPENDIX: EXAMPLE EXPRESSION FOR THE COMPONENTS Ξ_{33}^{33} AND Λ_{33}^{0}

The individual components of $\boldsymbol{\Xi}$ may be written in terms of the coefficients K_0, K_1, and K_2. Analytical forms of the 44 independent components of $\boldsymbol{\Xi}$ for polycrystalline materials with a uniaxial stress σ_{33} was given in Kube and Turner.[22] As an example, the analytical form of the component $\Xi_{33}^{33} = K_0 + K_1\sigma_{33} + K_2\sigma_{33}^2$, where

$$K_0 = \frac{16\nu^2}{525},\quad K_1 = \frac{32\nu}{5775}\big[11s_{12}(\nu + d_1 + 3d_2 + 8d_3) + 6s_{44}(11\nu + 5d_1 + 11d_2 + 44d_3) + \nu_s(44c_{12} + 88c_{44} + 49\nu + 44c_{144} + 88c_{456} + 15d_1 + 33d_2 + 164d_3)\big],\ \text{and}$$

$$K_2 = \frac{16}{525525}\Big\{\nu_s^2\big[20081\nu^2 + 728c_{12}(22c_{12} + 88c_{44} + 49\nu + 44c_{144} + 88c_{456} + 15d_1 + 33d_2 + 164d_3) + 1456c_{44}(44c_{44} + 49\nu + 44c_{144} + 88c_{456} + 15d_1 + 33d_2 + 164d_3) + 728c_{144}(49\nu + 22c_{144} + 88c_{456} + 15d_1 + 33d_2 + 164d_3) + 1456c_{456}(49\nu + 44c_{456} + 15d_1 + 33d_2 + 164d_3) + 15d_1(818\nu + 125d_1 + 546d_2 + 2728d_3) + 273d_2(33d_2 + 328d_3 + 98\nu) + 8d_3(16729\nu + 27922d_3)\big] + s_{12}\nu_s\big[182\nu(44c_{12} + 88c_{44} + 49\nu) + 8008(c_{12} + 2c_{44} + c_{144} + 2c_{456})(d_1 + 3d_2 + 8d_3) + 728\nu(11c_{144} + 22c_{456} + 16d_1 + 45d_2 + 139d_3) + 182(15d_1 + 33d_2 + 164d_3)(d_1 + 3d_2 + 8d_3)\big] + s_{44}\nu_s\big[1092\nu(44c_{12} + 88c_{44} + 49\nu) + 4368(c_{12} + 2c_{44} + c_{144} + 2c_{456})(5d_1 + 11d_2 + 44d_3) + 24\nu(2002c_{144} + 4004c_{456} + 1705d_1 + 3731d_2 + 16380d_3) + 7500d_1^2 + 36036d_2^2 + 716352d_3^2 + 32760d_1d_2 + 147360d_1d_3 + 323232d_2d_3\big] + 1001s_{12}^2(\nu + d_1 + 3d_2 + 8d_3)^2 + 1092s_{12}s_{44}(\nu + d_1 + 3d_2 + 8d_3)(11\nu + 5d_1 + 11d_2 + 44d_3) + 12s_{44}^2\big[625d_1^2 + 2730d_1(\nu + d_2 + 4d_3) + 3003(\nu + d_2 + 4d_3)^2\big]\Big\}. \tag{A1}$$

TABLE III. Acoustoelastic coefficients of aluminum C_0 (GPa) and C_1 (dimensionless units) calculated from the single-crystal elastic constants in Table I.

	Λ^0_{11}	Λ^0_{12}	Λ^0_{13}	Λ^0_{33}	Λ^0_{44}	Λ^0_{66}
C_0	112.240	59.880	59.880	112.240	26.180	26.180
C_1	1.659	0.1771	−1.115	−10.705	−1.704	0.7409

The coefficients K_0, K_1, and K_2 are functions of the second- and third-order single-crystal elastic constants where $d_1 = c_{111} - 3c_{112} + 2c_{123} + 12c_{144} - 12c_{155} + 16c_{456}$, $d_2 = c_{112} - c_{123} - 2c_{144}$, $d_3 = c_{155} - c_{144} - 2c_{456}$, $\nu = c_{11} - c_{12} - 2c_{44}$, $\nu_s = s_{11} - s_{12} - 2s_{44}$, $s_{11} = (c_{11} + c_{12})/[(c_{11} - c_{12})(c_{11} + 2c_{12})]$, $s_{12} = -c_{12}/[(c_{11} - c_{12})(c_{11} + 2c_{12})]$, and $s_{44} = 1/(4c_{44})$. For this component, $K_0 = 3.42$ GPa^2, $K_1 = -3.16$ GPa, and $K_2 = 2.34$, where the single-crystal elastic constants from Table I were used to evaluate Eq. (A1). All 44 independent components of Ξ for aluminum are given in Table II.

The analytical form of the stress-dependent tensor Λ^0 was given in Kube *et al.*[42] Each component of Λ^0 can be written in a linear form as a function of the uniaxial stress $\Lambda^0_{ijkl} = C_0 + C_1\sigma_{33}$. For the component $\Lambda^0_{IJ} = \Lambda^0_{33}$, the components C_0 and C_1 are

$$C_0 = c_{12} + 2c_{44} + \frac{3\nu}{5},$$

$$C_1 = \frac{1}{35}[\nu_s(49c_{12} + 98c_{44} + 39\nu + 35c_{123} + 154c_{144} + 168c_{456} + 15d_1 + 63d_2 + 204d_3) + 7s_{12}(5c_{12} + 10c_{44} + 3\nu + 15c_{123} + 50c_{144} + 40c_{456} + 3d_1 + 19d_2 + 44d_3) + 2s_{44}(105c_{12} + 420c_{44} + 63\nu + 35c_{123} + 210c_{144} + 280c_{456} + 15d_1 + 63d_2 + 252d_3)]. \quad \text{(A2)}$$

Values of the components of Λ^0 for aluminum are given in Table III using the single-crystal elastic constants from Table I.

[1]D. I. Crecraft, "The measurement of applied and residual stresses in metals using ultrasonic waves," J. Sound Vib. **5**, 173–192 (1967).
[2]D. M. Egle and D. E. Bray, "Measurement of acoustoelastic and third-order elastic constants for rail steel," J. Acoust. Soc. Am. **60**, 741–744 (1976).
[3]G. S. Kino, J. B. Hunter, G. C. Johnson, A. R. Selfridge, D. M. Barnett, G. Herrmann, and C. R. Steele, "Acoustoelastic imaging of stress fields," J. Appl. Phys. **50**, 2607–2613 (1979).
[4]G. S. Kino, D. M. Barnett, N. Graeli, G. Herrmann, J. B. Hunter, D. B. Ilic, G. C. Johnson, R. B. King, M. P. Scott, J. C. Shyne, and C. R. Steele, "Measurement of acoustoelastic and third-order elastic constants for rail steel," J. Nondestruct. Eval. **1**, 67–77 (1980).
[5]R. B. King and C. M. Fortunko, "Determination of in-plane residual stress states in plates using horizontally polarized shear waves," J. Appl. Phys. **54**, 3027–3035 (1983).
[6]R. B. Thompson, J. F. Smith, and S. S. Lee, "Microstructure-independent acoustoelastic measurement of stress," Appl. Phys. Lett. **44**, 296–298 (1984).
[7]T. Bateman, W. P. Mason, and H. J. McSkimin, "Third-order elastic moduli of germanium," J. Appl. Phys. **32**, 928–936 (1961).
[8]A. Seeger and O. Buck, "Die experimentelle Ermittlung der elastischen Konstanten höherer Ordnung" ("The experimental determination of higher-order elastic constants"), Z. Naturforsch. A **15**, 1056–1067 (1960).
[9]R. N. Thurston and K. Brugger, "Third-order elastic constants and the velocity of small amplitude waves in homogeneously stressed media," Phys. Rev. **133**, A1604–A1610 (1964).
[10]R. N. Thurston, "Effective elastic coefficients for wave propagation in crystals under stress," J. Acoust. Soc. Am. **37**, 348–356 (1965).
[11]R. E. Green, "Ultrasonic Investigation of Mechanical Properties," in *Treatise on Materials Science and Technology* (Academic Press, New York 1973).
[12]Y.-H. Pao, W. Sachse, and H. Fukuoka, "Acoustoelasticity and ultrasonic measurements of residual stress," in *Physical Acoustics*, edited by W. P. Mason and R. N. Thurston (Academic Press, New York 1984), Vol. 17, pp. 61–143.
[13]M. Hirao and H. Ogi, *EMATs for Science and Industry: Noncontacting Ultrasonic Measurements* (Kluwer Academic Publishers, Norwell, MA, 2003), pp. 215–260.
[14]A. Hikata, R. Truell, A. Granato, B. Chick, and K. Lücke, "Sensitivity of ultrasonic attenuation and velocity changes to plastic deformation and recovery in aluminum," J. Appl. Phys. **27**, 396–404 (1956).
[15]A. Hikata, B. Chick, C. Elbaum, and R. Truell, "Ultrasonic attenuation and velocity data on aluminum single crystals as a function of deformation and orientation," Acta Met. **10**, 423–429 (1962).
[16]A. Hikata, B. Chick, and C. Elbaum, "Effect of dislocations on finite amplitude waves in aluminum," Appl. Phys. Lett. **3**, 195–197 (1963).
[17]R. Truell, C. Elbaum, and B. B. Chick, *Ultrasonic Methods in Solid State Physics* (Academic Press, New York, 1969), pp. 230–251.
[18]H. Ogi, N. Suzuki, and M. Hirao, "Noncontact ultrasonic spectroscopy on deforming polycrystalline copper: Dislocation damping and acoustoelasticity," Metall. Mater. Trans. A **29**, 2987–2993 (1998).
[19]J. A. Turner and G. Ghoshal, "Polycrystals under applied loads," Appl. Phys. Lett. **97**, 031907 (2010).
[20]C. M. Kube, H. Du, G. Ghoshal, and J. A. Turner, "Stress-dependent changes in the diffuse ultrasonic backscatter coefficient in steel: Experimental results," J. Acoust. Soc. Am. **132**, EL43–EL48 (2012).
[21]C. M. Kube, H. Du, G. Ghoshal, and J. A. Turner, "Measurement of thermally induced stresses in continuously welded rail through diffuse ultrasonic backscatter," in *Review of Progress in Quantitative Nondestructive Evaluation*, edited by D. O. Thompson and D. E. Chimenti (AIP, Melville, NY, 2012), Vol. 31, pp. 1673–1680.
[22]C. M. Kube and J. A. Turner, "Stress-dependent second-order grain statistics of polycrystals," J. Acoust. Soc. Am. **138**, 2613–2625 (2015).
[23]G. Ghoshal, J. A. Turner, and R. L. Weaver, "Wigner distribution function of a transducer beam pattern within a multiple scattering formalism for heterogeneous solids," J. Acoust. Soc. Am. **122**, 2009–2021 (2007).
[24]G. Ghoshal and J. A. Turner, "Diffuse ultrasonic backscatter at normal incidence through a curved interface," J. Acoust. Soc. Am. **128**, 3449–3458 (2010).
[25]P. Hu, C. M. Kube, L. W. Koester, and J. A. Turner, "Mode-converted diffuse ultrasonic backscatter," J. Acoust. Soc. Am. **134**, 982–990 (2013).
[26]C. M. Kube, "Acoustoelastic scattering and attenuation in polycrystalline materials," Ph.D. dissertation, University of Nebraska-Lincoln, Lincoln, NE (2014).
[27]C.-S. Man and W. Y. Lu, "Towards an acoustoelastic theory for measurement of residual stress," J. Elast. **17**, 159–182 (1987).

[28]C.-S. Man and R. Paroni, "On the separation of stress-induced and texture-induced birefringence in acoustoelasticity," J. Elast. **45**, 91–116 (1996).
[29]C.-S. Man, "Effects of crystallographic texture on the acoustoelastic coefficients of polycrystals," Nondestruct. Test. Eval. **15**, 191–214 (1999).
[30]R. Paroni and C.-S. Man, "Constitutive equations of elastic polycrystalline materials," Arch. Rational Mech. Anal. **150**, 153–177 (1999).
[31]R. Paroni and C.-S. Man, "Two micromechanical models in acoustoelasticity: A comparative study," J. Elast. **59**, 145–173 (2000).
[32]M. Huang, H. Zhan, X. Lin, and H. Tang, "Constitutive relation of weakly anisotropic polycrystal with microstructure and initial stress," Acta. Mech. Sin. **23**, 183–198 (2007).
[33]The eighth-rank covariance tensor is written in Voigt's contracted index form when explicit components are expressed where the pairs of indices assume the following values: $11 \rightarrow 1$, $22 \rightarrow 2$, $33 \rightarrow 3$, 12 or $21 \rightarrow 6$, 13 or $31 \rightarrow 5$, 23 or $32 \rightarrow 4$.
[34]G. Simmons and H. Wang, *Single Crystal Elastic Constants and Calculated Aggregate Properties* (MIT Press, Cambridge, MA, 1971).
[35]A. G. Every and A. K. McCurdy, "Second and higher-order elastic constants," in *Landolt-Börnstein Numerical Data and Functional Relationships in Science and Technology New Series Group III: Crystal and Solid State Physics*, edited by O. Madelung and D. F. Nelson (Springer-Verlag, Berlin, 1992), Vol. 29.
[36]J. H. Rose, "Ultrasonic backscattering from polycrystalline aggregates using time-domain linear response theory," in *Review of Progress in Quantitative NDE*, edited by D. O. Thompson and D. E. Chimenti (Plenum Press, New York, 1991), Vol. 10, pp. 1715–1720.
[37]J. H. Rose, "Ultrasonic backscatter from microstructure," in *Review of Progress in Quantitative NDE*, edited by D. O. Thompson and D. E. Chimenti (Plenum Press, New York, 1992), Vol. 11, pp. 1677–1684.
[38]J. A. Turner and R. L. Weaver, "Radiative transfer and multiple scattering of diffuse ultrasound in polycrystalline media," J. Acoust. Soc. Am. **96**, 3675–3683 (1994).
[39]F. J. Margetan, P. Haldipur, and R. B. Thompson, "Looking for multiple scattering effects in backscattered ultrasonic noise from jet-engine nickel alloys," in *Review of Progress in Quantitative NDE*, edited by D. O. Thompson and D. E. Chimenti (AIP, Melville, NY, 2005), Vol. 14, pp. 2129–2136.
[40]S. Hirsekorn, "Theoretical description of ultrasonic propagation and scattering phenomena in polycrystalline structures aiming for simulations on nondestructive materials characterization and defect detection," in *Proceedings of the 11th ECNDT Conference*, Prague (2014).
[41]Wave modes are denoted with the prefix *quasi-* because a stress-induced anisotropy *can* cause the shear wave displacement to not be transverse and the longitudinal wave displacement to not be parallel to the propagation direction. For some special propagation directions, known as pure-mode directions, the displacements of the shear and longitudinal waves are perpendicular and parallel to the propagation direction, respectively. In order to avoid confusion, this article does not drop the use of the prefix *quasi-* for the pure-mode cases.
[42]C. M. Kube and J. A. Turner, "On the acoustoelasticity of polycrystalline materials," J. Acoust. Soc. Am. **138**, 1498–1507 (2015).
[43]L. Thomsen, "Weak elastic anisotropy," Geophysics **51**, 1954–1966 (1986).
[44]F. I. Fedorov, *Theory of Elastic Waves in Crystals* (Plenum Press, New York, 1968), pp. 217–226.
[45]J. A. Turner, "Elastic wave propagation and scattering in heterogeneous, anisotropic media: Textured polycrystalline materials," J. Acoust. Soc. Am. **106**, 541–552 (1999).
[46]See supplementary material at http://dx.doi.org/10.1121/1.4941253 for animated Figs. 3 and 4.
[47]R. L. Weaver, "Diffusivity of ultrasound in polycrystals," J. Mech. Phys. Solids **38**, 55–86 (1990).
[48]R. B. Thompson, F. J. Margetan, P. Haldipur, L. Yu, A. Li, P. Panetta, and H. Wasan, "Scattering of elastic waves in simple and complex polycrystals," Wave Motion **45**, 655–674 (2008).
[49]L. Yang and S. I. Rokhlin, "Ultrasonic backscattering in cubic polycrystals with ellipsoidal grains and texture," J. Nondestruct. Eval. **32**, 142–155 (2013).
[50]J. Li, L. Yang, and S. I. Rokhlin, "Effect of texture and grain shape on ultrasonic backscattering in polycrystals," Ultrasonics **54**, 1789–1803 (2014).